Supporting Information

Low-temperature N-anchored ordered Pt_3Co intermetallic nanoparticles as electrocatalysts for methanol oxidation reaction

Yanru Li [a, b ‡], *Hongwei Li* [a, b ‡], *Guixian Li* [a, b], *Dongliang Wang* [a, b], *Shoudeng Wang* [a, b], *Xinhong Zhao* [a, b, *]

a School of Petrochemical Technology, Lanzhou University of Technology, Lanzhou, 730050, China

b Key Laboratory of Low Carbon Energy and Chemical Engineering of Gansu Province, Lanzhou, 730050, China

* Corresponding author: College of Petrochemical Technology, Lanzhou University of Technology, 36 Pengjiaping Road, Lanzhou, Gansu Province, 730050, China. E-mail: licpzhaoxh@lu126.com (XH. Zhao)

‡ Yanru Li and Hongwei Li contributed equally to this paper

DFT Computational Method

The DFT calculations were conducted based on the Vienna Ab-inito Simulation Package (VASP)[1, 2]. The electron-ion interactions were described by the Projected Augmented-Wave (PAW) potentials, while the exchange-correlation interactions were calculated by employing the Perdew-Burke-Enzerhof (PBE) pseudopotentials of Generalized Gradient Approximation (GGA)[3, 4]. The PAW and PBE exchange-correlation functional supplied with the VASP package were employed for C ($2s^2 2p^2$ 08Apr2002), N ($2s^2 2p^3$ 08Apr2002), Pt ($5d^9 6s^1$ 04Feb2005) and Co ($3d^7 4s^2$ 02Aug2007). For structural optimization, the kinetic energy cutoff of the plane wave basis set was chosen to be 520 eV and the Brillouin zone integration is performed with 2×2×1 k points. An energy tolerance of 1.0×10-6 eV, and a maximum displacement of 1.0×10-2Å were considered.

The vdW-D3 method developed by Grimme was employed to describe the van der Waals interaction[5]. The plane-wave energy cutoff was set as 520 eV. The convergence threshold was set as 1.0×10-6 eV in energy and 0.01 eV per Angstrom in force. A four-layer face centered cubic structure of the Pt (111) or Pt_3Co (111) was adopted in which the lattice constant was chosen from Materials Project[6]. A vacuum layer of 15 Å was adopted to avoid the periodic interactions and the bottom two layers were fixed in order to increase the calculation efficiency. The Brillouin zone was modeled by gamma centered Monkhorst-Pack scheme, in which a 3×3×1 grid was adopted. Each electrochemical reaction step of methanol oxidation involves a ($H^+ + e^-$) pair transfer from the adsorbed species on the surface to the electrolyte.

The change in the Gibbs free energy of each ($H^+ + e^-$) pair transfer reaction was calculated by computational hydrogen electrode (CHE) model:

$$\Delta G = \Delta E_{pot} + \Delta E_{ZPE} - T\Delta S$$

In which the ΔE_{pot}, ΔE_{ZPE} and the ΔS were referred to as the change in potential energy, the change in the zero-point energy and the change in the entropy.

The zero-point energy was calculated by the summation of all vibrational frequencies:

$$E_{ZPE} = \frac{1}{2}\sum h\upsilon$$

where the ν corresponded to the vibriational frequency of each normal model[7].

References

[1] Kresse G, Furthmüller J. Efficiency of ab-initio total energy calculations for metals and semiconductors using a plane-wave basis set. Comp. Mater. Sci. **1996**, 6, 15-50.

[2] Kresse G, Furthmüller J. Efficient iterative schemes for ab initio total-energy calculations using a plane-wave basis set. Phys. Rev. B. **1996**, 54, 11169-11186.

[3] Blöchl PE. Projector augmented-wave method. Phys. Rev. B. 50 (**1994**) 17953-17979.

[4] Perdew JP, Burke K, Ernzerhof M. Generalized Gradient Approximation Made Simple [Phys. Rev. Lett. 77, 3865 (1996)]. Phys. Rev. Lett. **1997**, 78, 1396-1396.

[5] Grimme S, Antony J, Ehrlich S, et al. A consistent and accurate ab initio parametrization of density functional dispersion correction (DFT-D) for the 94 elements H-Pu. J. Chem. Phys., **2010**, 132, 154104.

[6] Jain A, Ong S P, Hautier G, et al. Commentary: The Materials Project: A materials genome approach to accelerating materials innovation. APL materials, **2013**, 1, 011002.

[7] Li Y, Chan S H, Sun Q. Heterogeneous catalytic conversion of CO_2: a comprehensive theoretical review. Nanoscale. **2015**, 7, 8663-8683.

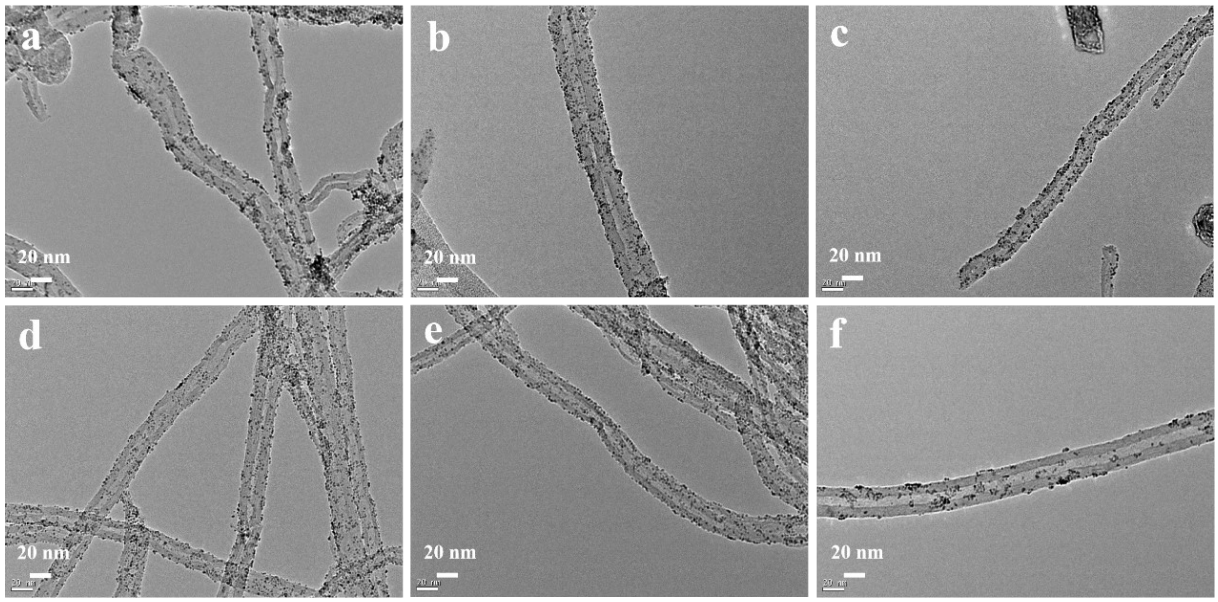

Figure S1. Different TEM images of a) Pt_3Co/N-CNT-U, b) Pt_3Co/N-CNT-M, c) Pt_3Co/N-CNT-P, d) Pt_3Co/N-CNT-T, e) Pt_3Co/N-CNT-H, and f) Pt_3Co/CNTs.

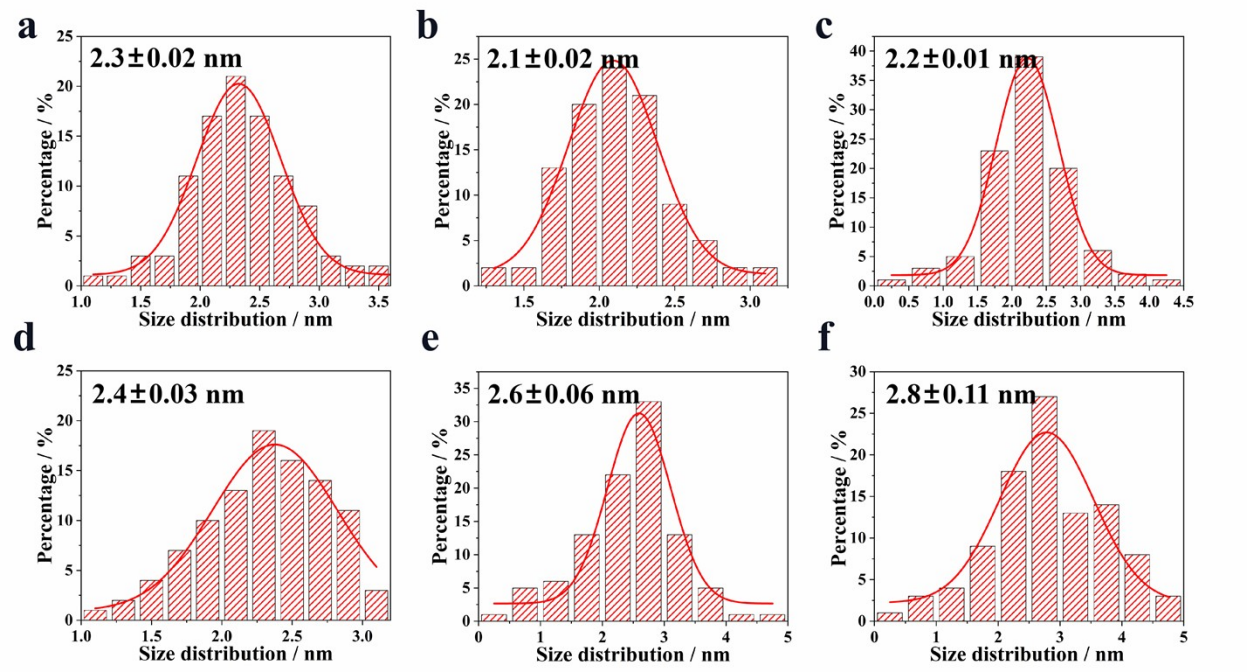

Figure S2. Particle size distribution histograms of Pt_3Co supported on a) N-CNT-U, b) N-CNT-M, c) N-CNT-P, d) N-CNT-T, e) N-CNT-H, and f) CNTs.

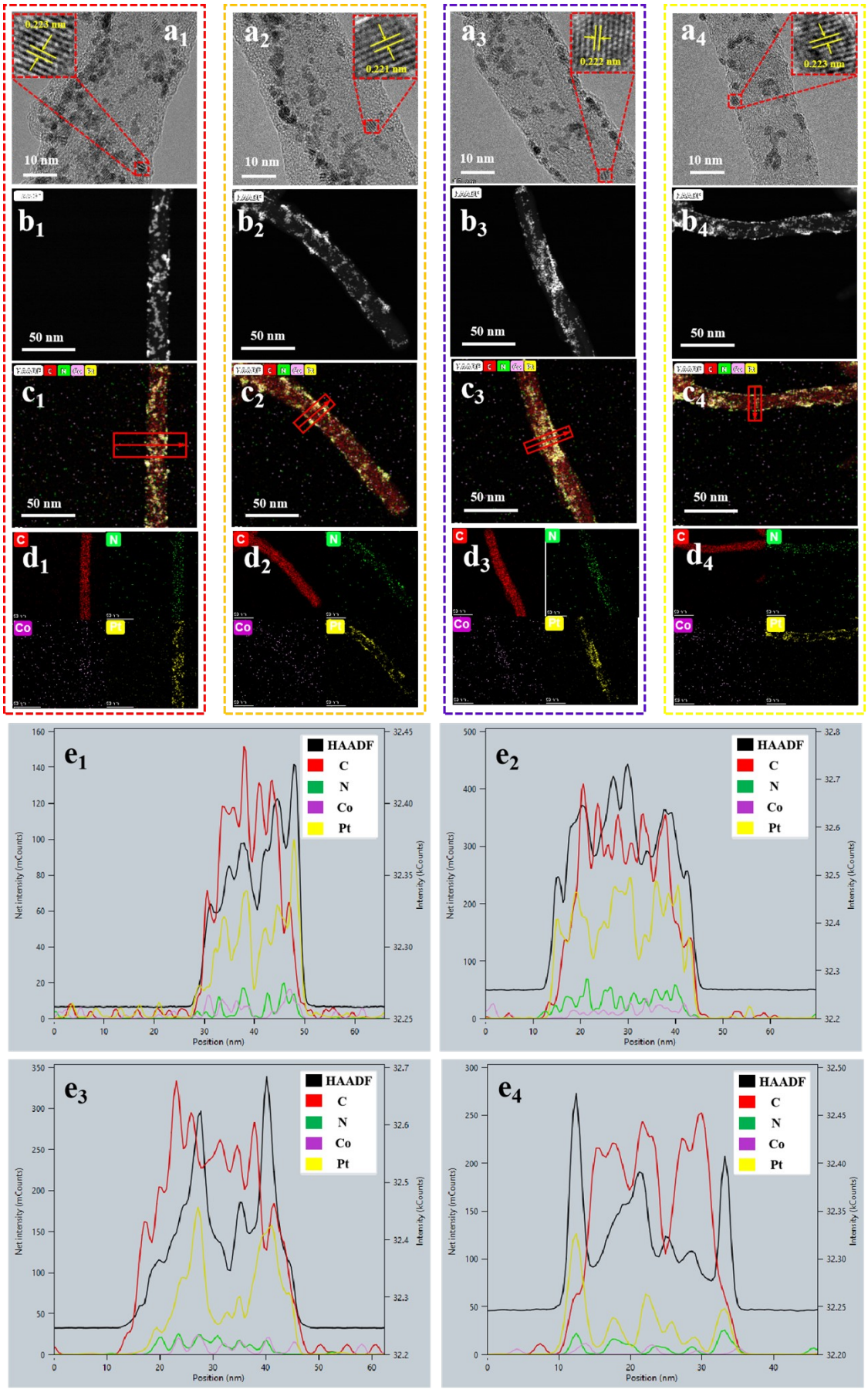
a1
a2
a3
a4
0.223 nm
0.221 nm
0.222 nm
0.223 nm
10 nm
b1
b2
b3
b4
50 nm
c1
c2
c3
c4
d1
d2
d3
d4
C
N
Co
Pt
e1
e2
e3
e4
HAADF
Net intensity (mCounts)
Intensity (kCounts)
Position (nm)

Figure S3. Structural and compositional characterizations of Pt_3Co/N-CNT-U (a_1-e_1), Pt_3Co/N-CNT-P (a_2-e_2), Pt_3Co/N-CNT-T (a_3-e_3) and Pt_3Co/N-CNT-H (a_4-e_4). $a_{1\text{-}4}$) HRTEM; $b_{1\text{-}4}$) HAADF-STEM images; $c_{1\text{-}4}$), $d_{1\text{-}4}$) EDX elemental mapping images; $e_{1\text{-}4}$) Elemental surface scans of area in $c_{1\text{-}4}$; The inset in ($a_{1\text{-}4}$) is the enlarged HRTEM image of the selected area. The N, C, Co and Pt atoms are in green, red, purple and yellow colors, respectively.

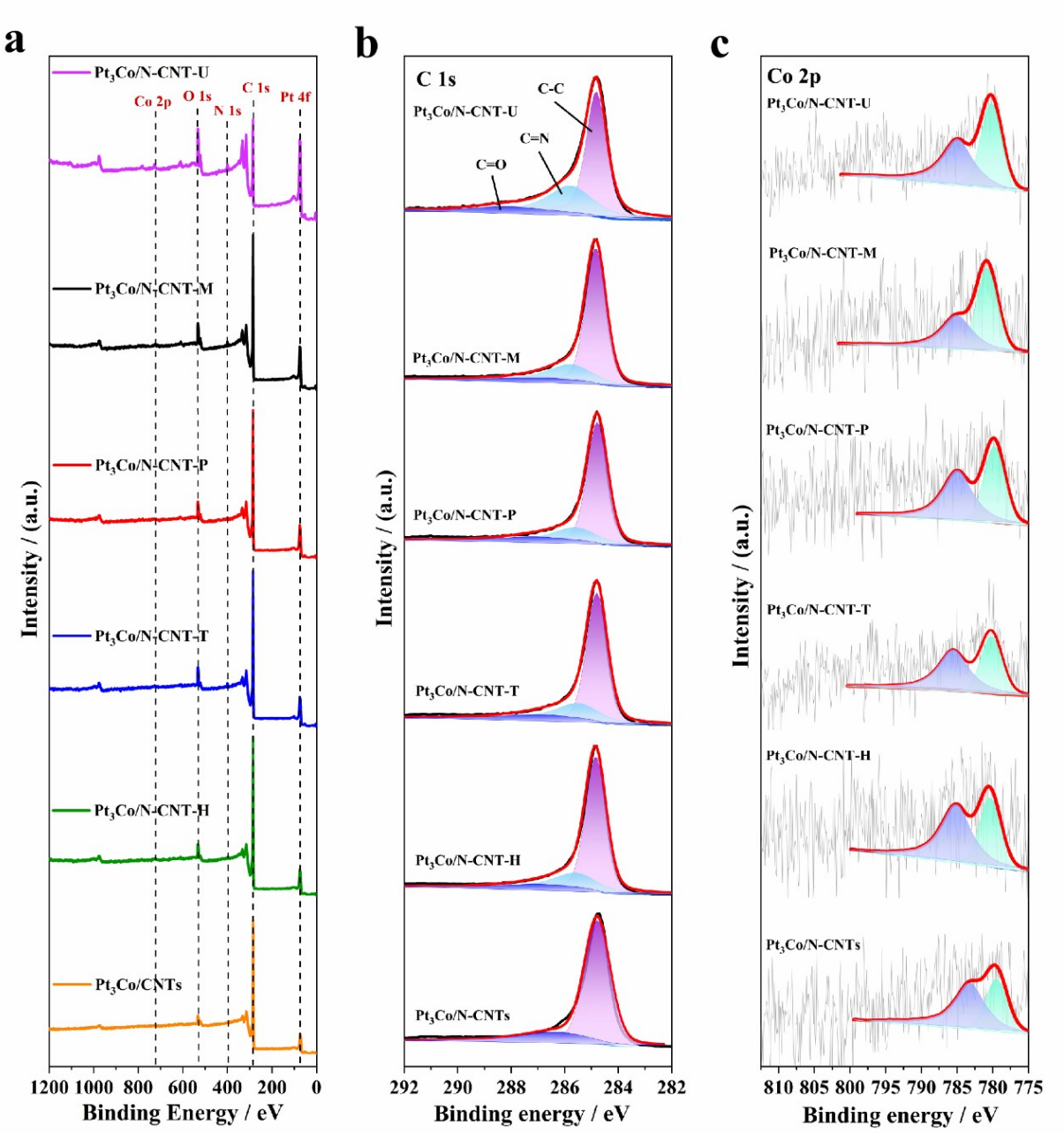

Figure S4. XPS patterns for a) survey; b) C 1s; c) Co 2p regions of Pt_3Co/N-CNT-U, Pt_3Co/N-CNT-M, Pt_3Co/N-CNT-P, Pt_3Co/N-CNT-T, Pt_3Co/N-CNT-H, and Pt_3Co/CNTs.

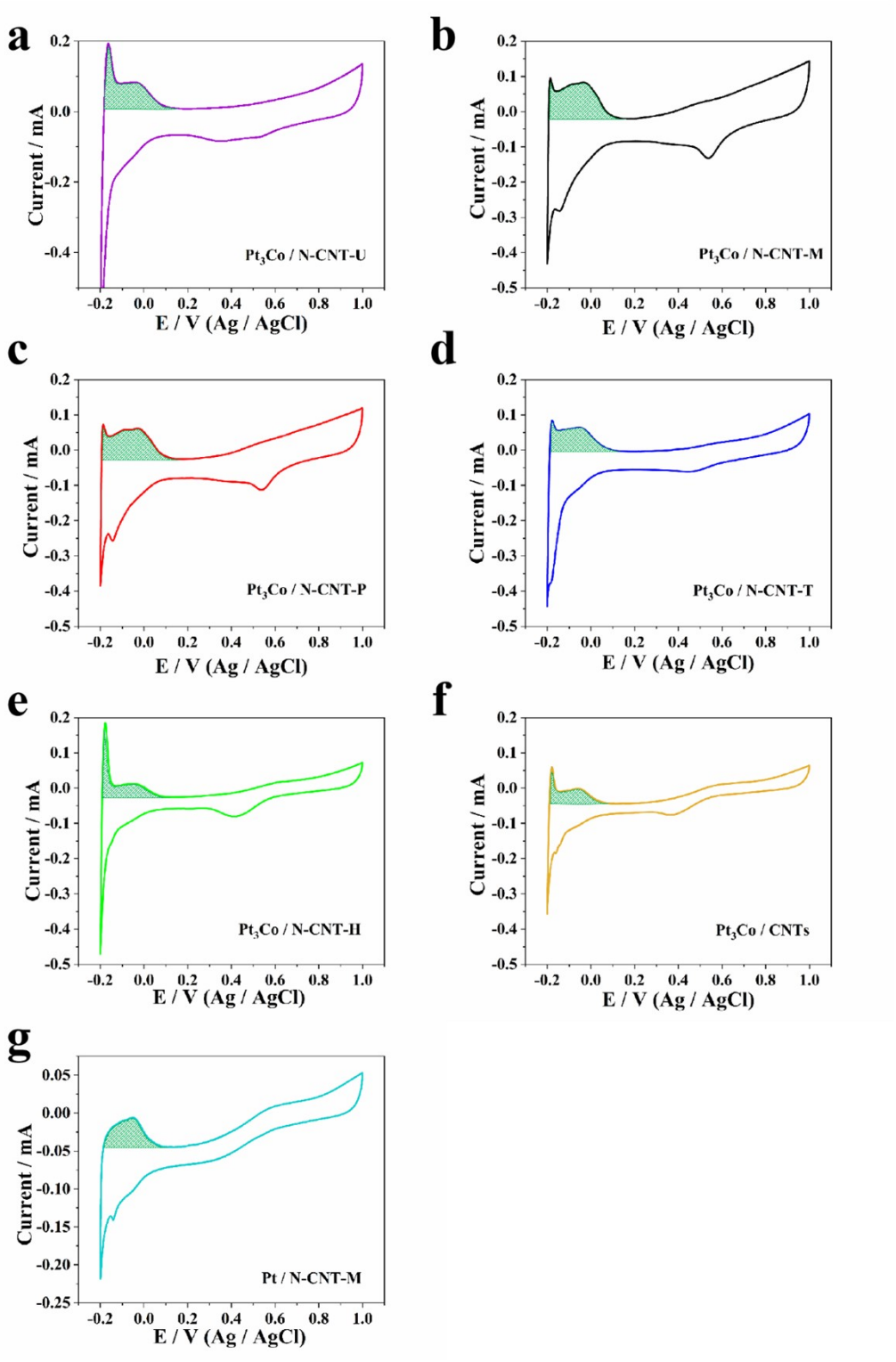

Figure S5. Hydrogen desorption domains of a) Pt_3Co/N-CNT-U; b) Pt_3Co/N-CNT-M; c) Pt_3Co/N-CNT-P; d) Pt_3Co/N-CNT-T; e) Pt_3Co/N-CNT-H; f) Pt_3Co/CNTs, and g) Pt/N-CNT-M.

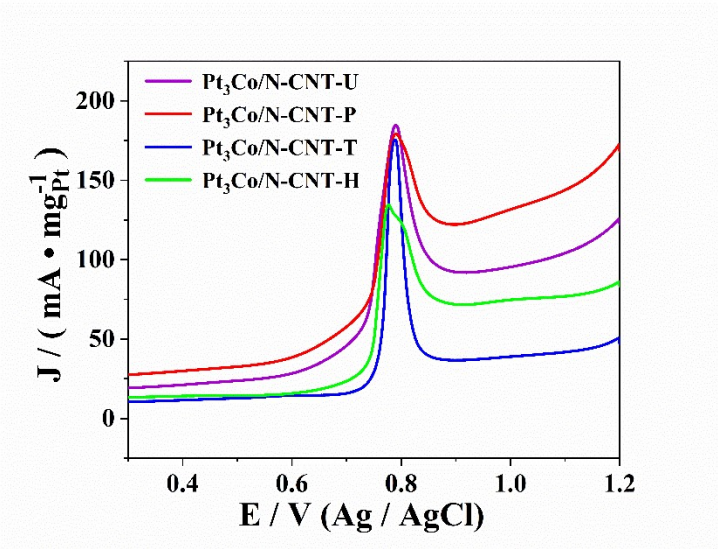

Figure S6. CO-stripping voltammograms of Pt_3Co/N-CNT (U, P, T, H) at a scan rate of 50 mV s^{-1} in 0.5 M H_2SO_4.

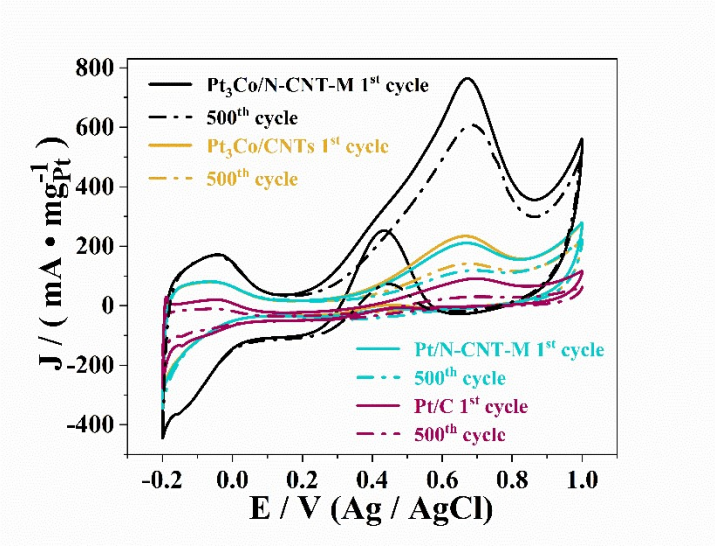

Figure S7. CVs of Pt_3Co/N-CNT-M, Pt_3Co/CNTs, Pt/N-CNT-M, and commercial Pt/C before and after 500 potential cycles.

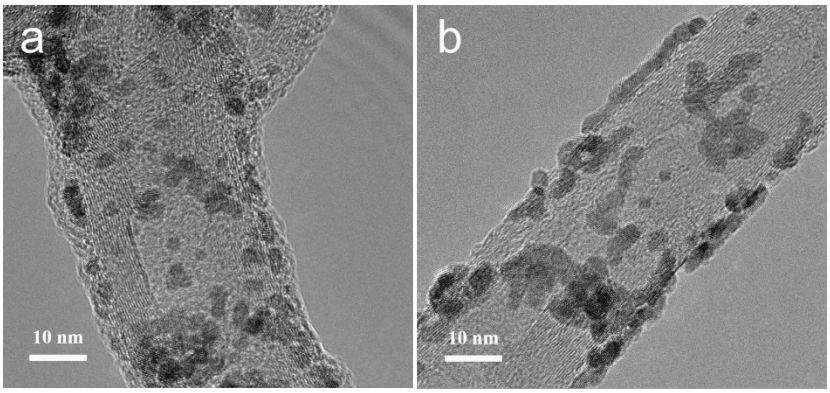

Figure S8. TEM images of the Pt_3Co/N-CNT-M before (a) and after (b) durability test.

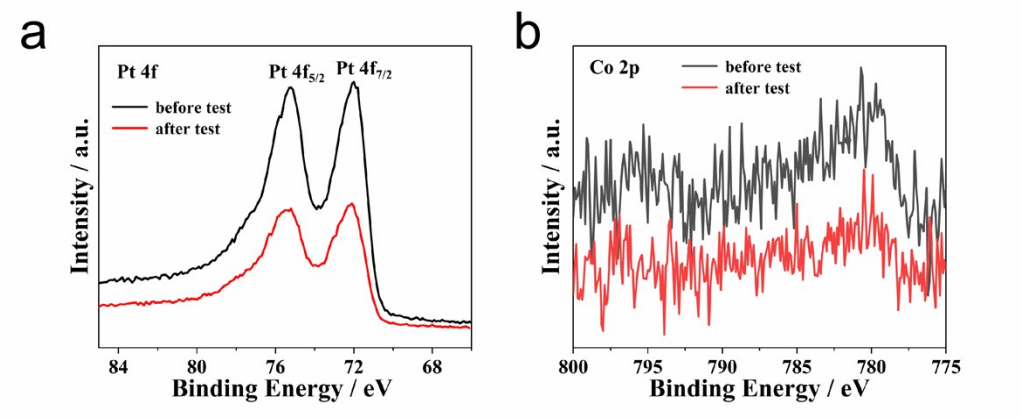

Figure S9. Comparison of XPS spectra of the Pt_3Co/N-CNT-M before and after durability test.

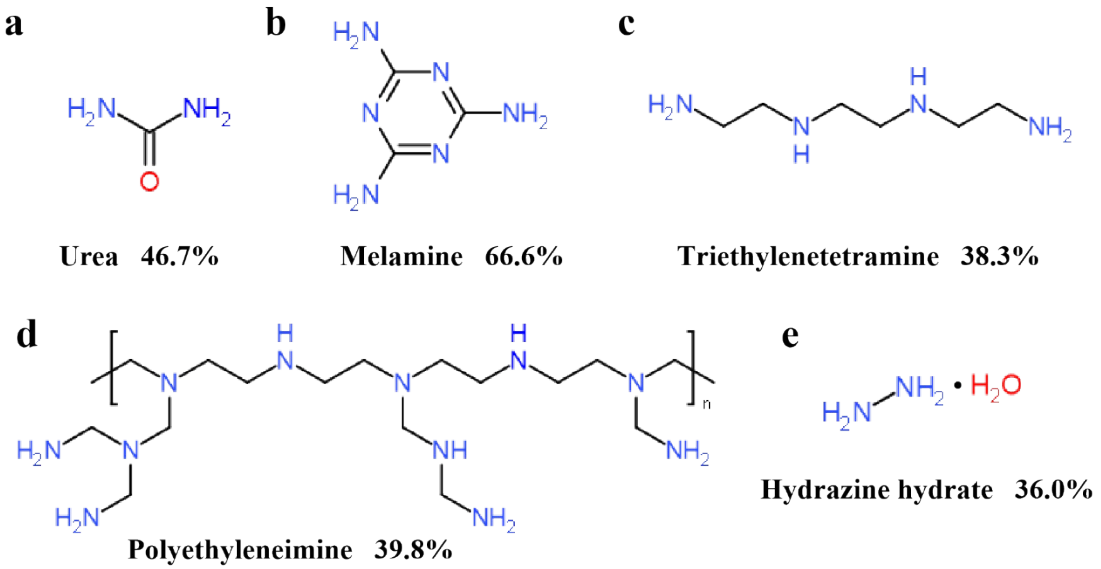

Figure S10. The structural formula and N content for a) urea; b) melamine; d) polyethyleneimine; c) triethylenetetramine; and e) hydrazine hydrate.

Table S1. TGA, Raman and ICP-OES results of Pt_3Co NPs supported on N-CNT-U, N-CNT-M, N-CNT-P, N-CNT-T, N-CNT-H, and CNTs.

Samples	N doping (wt%)		Pt_3Co loading (wt%)	Decomposition temperature (°C)	Raman I_D/I_G	Pt:Co ratio by ICP-OES
N-CNT-U	[a]1.14	[b]1.08	17.7	380 ~ 545	1.26	4.01:1
N-CNT-M	1.21	1.19	18.7	410 ~ 572	1.35	3.92:1
N-CNT-P	0.95	0.83	18.8	410 ~ 575	1.37	3.95:1
N-CNT-T	0.62	0.60	14.5	410 ~ 570	1.31	3.86:1
N-CNT-H	0.65	0.55	18.5	410 ~ 610	1.32	3.90:1
CNTs	-		10.8	280 ~ 550	1.23	3.84:1

[a] The TGA data.

b The elemental analysis test data.

Table S2. Surface areas, pore volumes and pore size distribution of N-CNT-U, N-CNT-M, N-CNT-P, N-CNT-T, N-CNT-H, and CNTs.

Samples	SBET ($m^2 \cdot g^{-1}$)	V_{micro} ($cm^3 \cdot g^{-1}$)	V_{meso} ($cm^3 \cdot g^{-1}$)	V_{total} ($cm^3 \cdot g^{-1}$)
N-CNT-U	141.1	0.003	0.815	0.818
N-CNT-M	191.8	0.007	0.764	0.771
N-CNT-P	194.2	0.012	0.798	0.810
N-CNT-T	170.4	0.012	0.778	0.790
N-CNT-H	227.2	0.010	0.910	0.920
CNTs	110.0	0.003	0.680	0.683

Table S3. The amount of Pt^0 and Pt^{2+} for Pt_3Co/N-CNT (U, M, P, T, H), and Pt_3Co/CNTs.

Samples	Pt^0 (%)	Pt^{2+} (%)
Pt_3Co/N-CNT-U	70.9	29.1
Pt_3Co/N-CNT-M	74.5	25.5
Pt_3Co/N-CNT-P	70.6	29.4
Pt_3Co/N-CNT-T	69.5	30.5
Pt_3Co/N-CNT-H	69.4	30.6
Pt_3Co/CNTs	65.9	34.1

Table S4. ECSA, Current density, I_f/I_b, Initial potential, Mass and Specific activity of Pt_3Co/N-CNT (U, M, P, T, H), Pt_3Co/CNTs, and Pt/N-CNT-M.

Samples	ECSA ($m^2 \bullet g^{-1}$)	Current density ($mA \bullet mg^{-1}_{Pt}$)	I_f/I_b	Initial potential (eV)	Mass activity ($mA \bullet mg^{-1}_{Pt}$)	Specific activity ($mA \bullet cm^{-2}$)
Pt_3Co/N-CNT-U	183.46	742.2	1.46	0.23	742.2	5.91
Pt_3Co/N-CNT-M	213.17	767.8	2.95	0.20	767.8	6.11
Pt_3Co/N-CNT-P	183.78	528.2	1.80	0.23	528.2	4.20
Pt_3Co/N-CNT-T	132.36	353.4	2.19	0.25	353.4	2.81
Pt_3Co/N-CNT-H	113.57	310.4	3.30	0.26	310.4	2.47
Pt_3Co/CNTs	83.33	234.2	-	0.38	234.2	1.86
Pt/N-CNT-M	58.41	211.0	-	0.37	211.0	1.68
Pt/C	-	91.4	-	0.44	91.4	0.73

Table S5. DFT calculated binging energies of Pt_3Co on the surface of CNTs and N-CNT.

C	**Pt_3Co**	**C-Pt_3Co**	**Eads**
-6.66419770E+02	-1.61955060E+01	-6.83250090E+02	-6.34814000E-01
CN	Pt_3Co	CN-Pt_3Co	Eads
-6.41212860E+02	-1.61955060E+01	-6.63242610E+02	-5.83424400E+00

Table S6. Calculated Gibbs free energies (eV) of intermediates on Pt (111) surface for MOR.

Intermediates	VASP	Free energy correction	Corrected energy	Real free energy	ΔG	Relative G
CH_3OH*	-438.231	1.254	-436.977	-451.197	-	0.000
CH_2OH*	-434.694	0.993	-433.701	-451.321	-0.124	-0.124
CHOH*	-430.734	0.730	-430.004	-451.024	0.297	0.173
COH*	-427.483	0.363	-427.119	-451.539	-0.515	-0.342
CO*	-424.088	0.131	-423.957	-451.777	-0.238	-0.580
CO*+OH*	-434.196	0.390	-433.806	-450.806	0.971	0.391
CO_2	-430.309	-0.257	-430.567	-450.967	-0.161	0.230

Table S7. Calculated Gibbs free energies (eV) of intermediates on Pt_3Co (111) surface for MOR.

Intermediates	VASP	Free energy correction	Corrected energy	Real free energy	ΔG	Relative G
CH_3OH*	-453.030	1.268	-451.762	-465.982	-	0.000
CH_2OH*	-448.588	1.044	-447.544	-465.164	0.819	0.819
CHOH*	-445.000	0.747	-444.253	-465.273	-0.109	0.709
COH*	-441.285	0.421	-440.864	-465.284	-0.011	0.698
CO*	-438.454	0.120	-438.334	-466.154	-0.870	-0.171
CO*+OH*	-449.025	0.438	-448.587	-465.587	0.566	0.395
CO_2	-444.748	-0.257	-445.005	-465.405	0.182	0.577